The Thesis Committee for Yingnan Liu
Certifies that this is the approved version of the following thesis:

Microwave Impedance Microscope Study of Two Dimensional Materials

APPROVED BY SUPERVISING COMMITTEE:

Supervisor: ______________________________
Keji Lai

____
Chih-Kang Shih

Microwave Impedance Microscope
Study of Two Dimensional Materials

by

Yingnan Liu, B.Nat.Sci.

Thesis

Presented to the Faculty of the Graduate School of

The University of Texas at Austin

in Partial Fulfillment

of the Requirements

for the Degree of

Master of Arts

The University of Texas at Austin

May 2015

Dedication

I would like to delicate this thesis to my parents, who always respect my choice and are very supportive during my entire life.

Acknowledgements

I am very grateful to my supervisor, Prof. Keji Lai. He has provided me many interesting research projects and help me published my first paper. I am also grateful to our postdoc, Dr. Yuan Ren, who has led me into this field and been patient to answer my questions.

I'd like to express my gratitude to my cooperators, Dr. Rudresh Ghosh, for his support and wonderful work and his supervisor, Prof. Rodney Ruoff, for his guidance.

I also want to express my gratitude to my other group members, Xiaoyu Wu, Dr. Di Wu, for their valuable discussion.

Abstract

Microwave Impedance Microscope
Study of Two Dimensional Materials

Yingnan Liu, MA
The University of Texas at Austin, 2015

Supervisor: Keji Lai

In this thesis, I will introduce a unique technique, microwave impedance microscope (MIM), which has shown its potential in characterization of local electrical inhomogeneity of materials. I will also discuss some results about the study of In_2Se_3 and MoS_2 electrical properties with MIM.

Table of Contents

List of Figures

Chapter 1: Introduction

Research of two dimensional (2D) materials has been an extremely attractive field since the isolation of graphene, a single atomic layer of carbon, from the bulk graphite. Extensive work has been done to explore their applications in nanoelectronics, optoelectronics, and novel untra-thin flexible devices, which are largely attributed to their atomic thickness, controllable electrical properties, transparency, flexibility, and other advantages over conventional three dimension materials.

Traditionally, transport measurement plays an importance role in characterizing electrical properties of materials. However, such transport measurements do not provide the spatially resolved information of electronic materials. A non-destructive in situ characterization tool to map out the local electrical conductivity is therefore critical to advance our understandings in this research field. In Prof. Lai's lab, we have take advantages of a unique scanning system, known as the microwave impedance microscopy (MIM), to take on this challenge.

In this thesis, I will show the principle and design of MIM as well as our earlier research results of 2D materials characterized by MIM.

Chapter 2: Microwave Impedance Microscopy

In this chapter, I will introduce the basic principle of MIM and numerical analysis of MIM results.

PRINCIPLE OF MIM

Shown in Figure 1(a) is a schematic of the MIM setup.[1] The 1GHz excitation V_{1GHz} ~ 20mV is sent to the cantilever through a Z-match section, which converts the tip impedance (C ~ 1.2 pF and R ~ 4 Ω) to 50 Ω. The red curve shown in Figure 1(b) depicts the reflection coefficient S_{11} from the Z-match section. The system is operated at the frequency of minimum S_{11}, which also corresponds to the maximum ΔS_{11}. During the scanning process, the near-field tip-sample interaction changes the effective impedance of the tip, rendering a change of the reflected microwave voltage $\Delta S_{11} \bullet V_{1GHz}$. The blue curve shown in Figure 1(b) depicts the calculated frequency-dependent ΔS_{11}, assuming an admittance change of 1nS. This RF input ($\Delta S_{11} \bullet V_{1GHz}$) is then amplified by an RF amplifier, and then demodulated by a mixer to be further amplified by a DC amplifier for the final output. Figure 1(c) shows the characteristic response of the amplifier. Experimentally, one needs to adjust the phase shifter in front of the mixer, such that the two orthogonal channels are aligned to the real and imaginary components of the tip-sample admittance.[1]

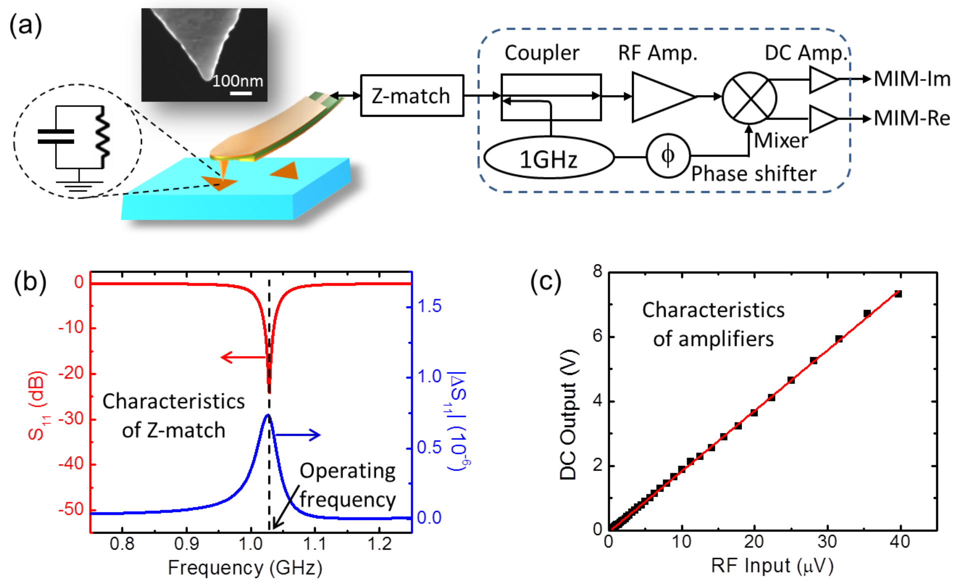

Figure 1: (a) Schematic of the MIM setup (b) Simulated reflection coefficient S_{11} (in red) and ΔS_{11} (in blue) (c) Amplifier Response

Modeling of Tip-sample Interaction

In order to quantitatively analyze MIM signals, finite element analysis (FEA) is used to model the tip-sample interaction. Here, commercial FEA software, COMSOL and its AC/DC module, was used. The procedure to model a monolayer MoS_2 sample is illustrated below as an example.

For a rotationally symmetric setup, the 2D-axisymmetric mode was chosen to reduce the computational time and calculate the high frequency quasi-static potential distribution between the two electrodes.[2] A cross section of the tip, sample, and their surrounding environment was simulated and assigned with the proper dielectric constants, electrical conductivities, and boundary conditions. For this specific example, the boundary condition at the tip has a signal of 1 V, while the surroundings away from sample is grounded (and therefore 0 V). The "finer" mesh size was selected here as a compromise between sample size, resolution, and calculation time. A parameter sweep was then calculated at 1 GHz to solve for the sample conductivity or permittivity. It should be noted that the real and imaginary parts of the tip-sample admittance, Y_{11}, is also obtained in this calculation.

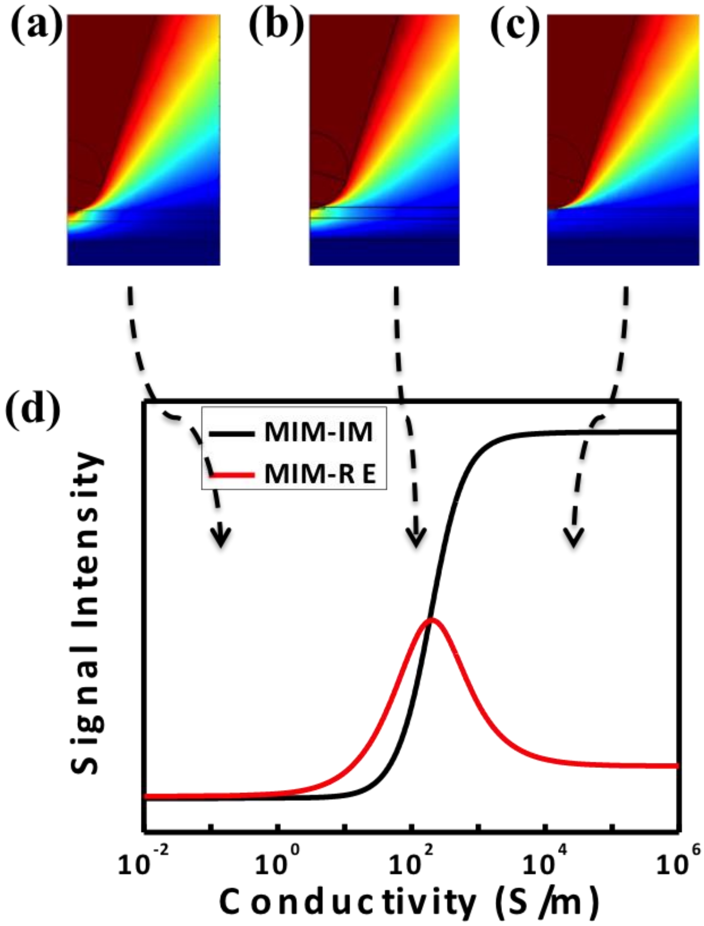

Figure 2: Typical simulation results of monolayer MoS_2 sample

Typical simulation results of a monolayer MoS_2 sample on Si/SiO_2 substrate are shown in Figure 2. The potential distribution around the tip and sample of the insulating regime, the semiconducting regime and the conducting regime are shown in Figure 2 (a), (b) ,and (c), respectively. When $\sigma < 1$ S/m (the insulating regime), both MIM-Im and MIM-Re signals are low. When the sample enters the semiconducting regime (σ ~1 S/m —10^4 S/m), signals in both channels start to increase. MIM-Re shows a peak at 5×10^2 S/m, when Re ($\Delta Z_{tip-sample}$)~Im ($\Delta Z_{tip-sample}$)[2]. When $\sigma > 10^4$ S/m (the conducting regime), a large signal is detectable in the MIM-Im channel while a very low signal is shown in MIM-Re. An estimation of the local conductivity requires taking the ratio between MIM-Im and MIM-Re signals. For accurate results, a calibration procedure on standards is strongly recommended prior to experimentation.

Chapter 3: Study of Two-dimensional Systems

MIM enables us to acquire local electrical information with sub-micrometer resolution of 2D systems. Such capabilities open up an array of explorative topics such as the characterization of such as defects, boundary structures, and interactions between the sample and the environment. In this chapter, two interesting studies are reported. The first one is the local electrical imaging of few-layers of indium selenide (In_2Se_3) and the corresponding changes of dielectric constants. The second one is the local electrical imaging of monolayer molybdenum disulphide (MoS_2) and the mapping of its dendritic structures.

Layer-dependent Dielectric Constant Study of In_2Se_3

The past decade has witnessed a dramatic increase of research interests on quasi-two-dimensional (q2D) layered materials. Among them, layered semiconductors have gained particular interest for their potential roles as channel materials. The bulk q2D materials possess many anisotropic physical properties, which can be explained by the weak van der Waals (vdW) interactions and strong intralayer covalent bonding. One can expect that the dielectric constant, which determines the capacitance and charge screening in electronic devices, can be strongly influenced by the number of layers (n) in a thin-flim q2D system.

Here, the layered semiconducting chalcogenide In_2Se_3, a q2D material widely applied in thermoelectric, memory and photoelectric devices,[3] will be discussed into details. With the growth conditions cautiously controlled and samples screened, only the semiconducting α-phase In_2Se_3 was investigated. The crystal structure of α-phase In_2Se_3 is shown in Figure 3.[4] The In_2Se_3 nano-flakes investigated in this thesis were grown on mica substrates by van der Waals epitaxy.[4]

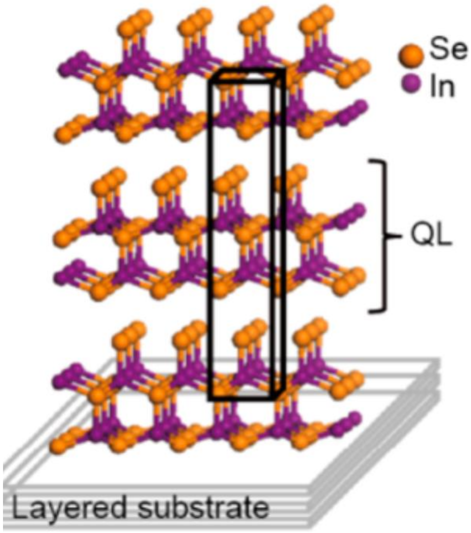

Figure 3: A crystal structure of In_2Se_3

The thickness and dielectric response of In_2Se_3 flakes was measured by MIM. Figure 4(a) and 4(b) exhibit the simultaneously taken topography and MIM images of several In_2Se_3 nano-flakes. The numbers in Figure 4(a) indicate the layer number with each In_2Se_3 quintuple layer about 1 nm thick. The MIM-Im image shows clearly that the contrast is a function of the flake thickness. For thin samples (n = 2 or 3), the MIM-Im signal is lower than that on the substrate, demonstrating a smaller dielectric constant of ultra-thin In_2Se_3 than that of mica ($\varepsilon_{r,\ mica} = 6$). Interestingly, the 4-layer regions of the corresponding flake are barely seen compared with background, while for n = 5, the corresponding regions are clearly visible. The MIM-Im signals intensities go well above that of mica substrate when flakes become thicker ($n \geq 6$), due to the relatively large bulk In_2Se_3 value of $\varepsilon_r = 17$ [5]. No signals above the noise level were detected in the MIM-Re channel during our measurement for all nano-flakes. Since MIM-Im gives relatively weak responses (<100mV), a conclusion can be drawn that rather than the negligible conductivity in the as-grown α-phase In_2Se_3, the microwave signal is solely induced by permittivity contrast over the substrate.

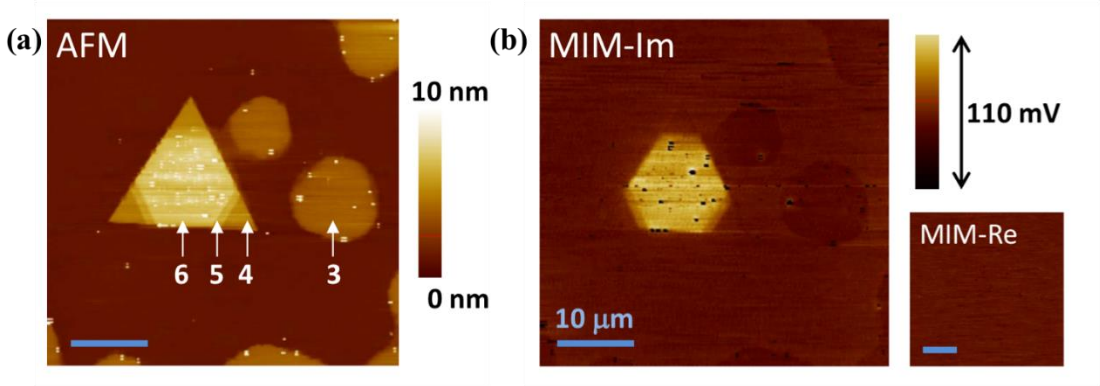

Figure 4: (a) Topography of In_2Se_3 flakes on mica. (b) MIM-Im and MIM-Re of the same region.

Figure 5 illustrate the quantitative analysis of the MIM data. A clear downward bend can be observed in Figure 5(a) at around 6 layers in the MIM-Im signals (blue), when the sample thickness decreases towards monolayer. Finite-element simulations using a numerical software COMSOL4.3 were carried out to interpret the results. Unfortunately, only the effective isotropic $\varepsilon_{r,eff}$ in In_2Se_3 can be extracted, rather than both in-plane and out-of-plane dielectric constants, due to the fact that the quasi-static electric field is nearly radial from the tip apex. The effective thickness-dependent $\varepsilon_{r,eff}$ was calculated based on the measured data and shown in Figure 5(b), from which a conclusion can be drawn that the dielectric constant increases steadily from 2 to 6 layers and then saturates to the bulk value. The simulated MIM-Im signals (red in Figure 5 (a)) with the effective $\varepsilon_{r,eff}$ match well with experimental results.

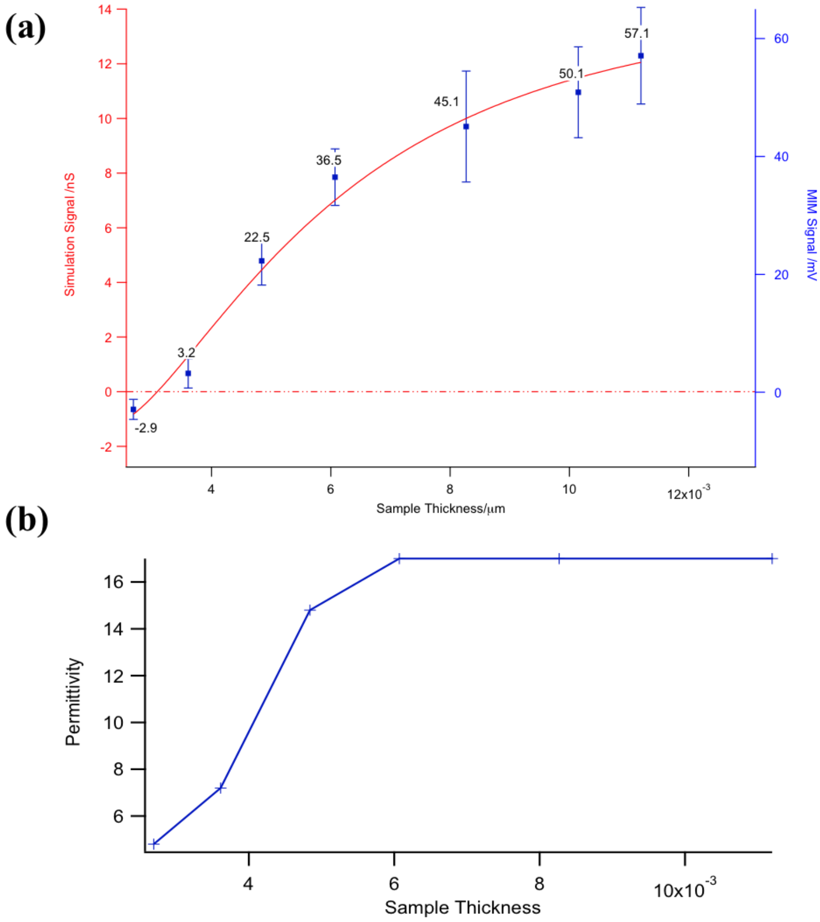

Figure 5: (a) Experimental and simulation results of different sample thickness. (b) Corresponding permittivity of different thicknesses.

IMAGING OF MoS_2 INHOMOGENEOUS CONDUCTIVITY

Single-layer molybdenum disulphide (MoS_2) is a direct band gap (E_g = 1.8eV) semiconductor with a thickness around 0.65 nm. An increasing number of reports demonstrate varies device prototypes, such as floating gate memories[6], photo detectors[7-8] and field-effect transistors [9-12], on exfoliated MoS_2 samples. The ability to produce large-area and high-quality monolayer MoS_2 films is an essential condition for its application in next generation nano-electronics. One way to evaluate the film quality is by evaluating the amount of imperfections on the chemically grown monolayer MoS2. Besides point defects, there also exist defects in the mesoscopic (nanometer to micrometer) length scale. In this thesis, I will report the electrical properties of those mesoscopic defects.

The crystal structure of MoS2 is shown in Figure 6[9].

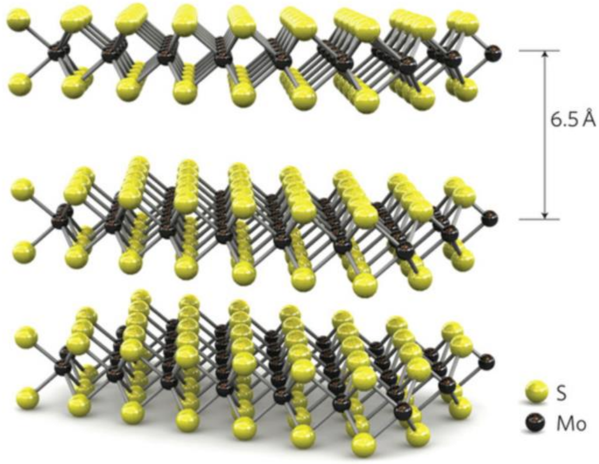

Figure 6: A crystal structure of MoS_2

The sulfurization of MoO_3 using chemical vapor deposition (CVD) has been used to prepare the MoS_2 films on SiO_2 (285 nm)/Si substrates.[13] The scanning electron microscopy (SEM) images were taken with different distances between the deposited film and the MoO_3 precursor and were illustrated in Figure 7(a) to (d). [1] Small isolated MoS_2 islands with a nearly round shape were observed in Figure 7(a) when the monolayer starts to grow. The flakes become bigger in size and more triangular in shape (Figure 7(b)) as they get closer towards the MoO_3 source. The neighboring grains were observed to start merging [Figure 7(c)] and eventually form a continuous film [Figure 7(d)] when the size of individual triangles reaches 30~50μm. Figure 7(e)[1] exhibits a random distribution of different sized dendritic precipitates within individual grains. The inset shows a clear structure of one ad-layer.[1]

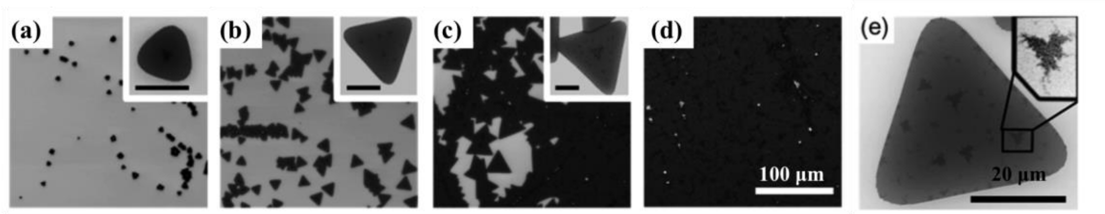

Figure 7: SEM images of CVD grown MoS_2

Raman and photoluminescence (PL) are used to characterize a single domain monolayer MoS_2 (shown in Figure 8 [1] (a) to (c)). Because of the sensitivity to inter-layer coupling, the Raman spectroscopy is a commonly used technique to determine the number of layers of 2D materials. A remarkable PL peak can be observed, which is due to the direct band gap in monolayer MoS_2. A far weaker PL signal and a wider E^1_{2g}-A_{1g} frequency separation compared with the monolayer MoS_2 background were seen from the Raman and PL maps of the dendritic regions. Combined with the atomic force microscopy [AFM, Fig. 8(d)] data, all conventional measurements (AFM, Raman, PL) suggest similar structure between the irregular ad-layers and MoS_2 bilayers.[1]

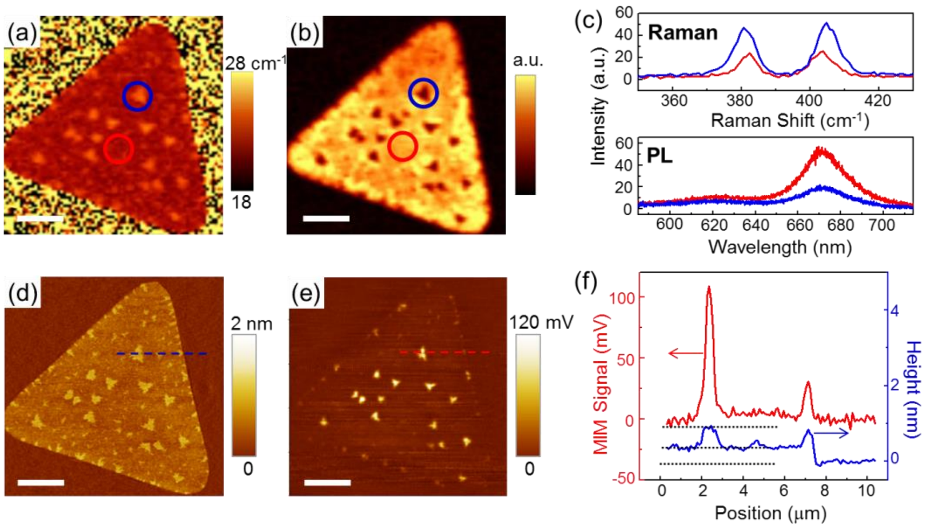

Figure 8: (a) Raman mapping of one MoS_2 flake. (b) Photoluminescence of the same region. (c) Raman and PL spectra for red and blue regions circled in (a) and (b). (d) AFM and (e) MIM-Im mapping of the same region. (f) Line cut of height (blue) and MIM-Im signals (red) in (d) and (e).

The local conductivity of the same MoS_2 atomic layers was studied by MIM and shown in Figure 8(e). The corresponding MIM signals of dendritic regions are dramatically larger than that on the monolayer MoS_2. Moreover, the line cut in Fig. 2(f) shows that bigger dendrites exhibit stronger MIM-Im signals.[1]

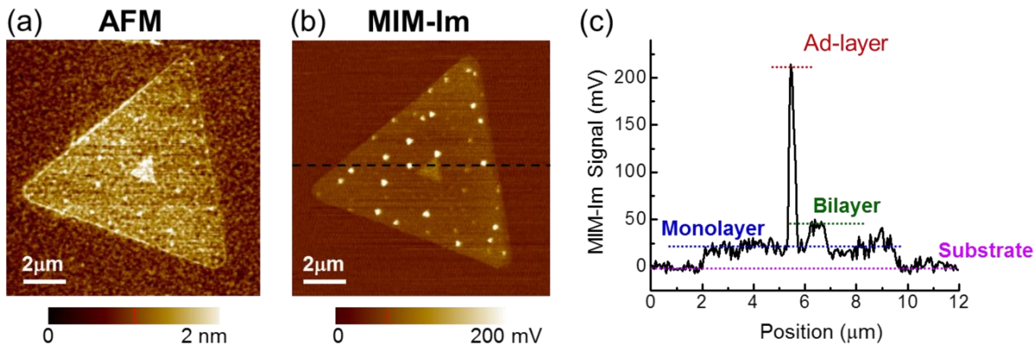

Figure 9: (a) AFM and (b) MIM-Im of a monolayer MoS_2 sample with dendritic structures and a bilayer island in the middle. (c) Line cut of MIM-Im signals in (b)

Interestingly, a triangular island with one extra layer thickness can be found in the middle of some MoS_2 samples. As shown in Figure 9[1], the MIM signals on these regularly shaped bilayers are twice as large as the monolayers while much lower than the dendritic ad-layers. The irregular dendrites are very different from regular well-crystalized triangular bilayers when considering the electrical properties.[1]

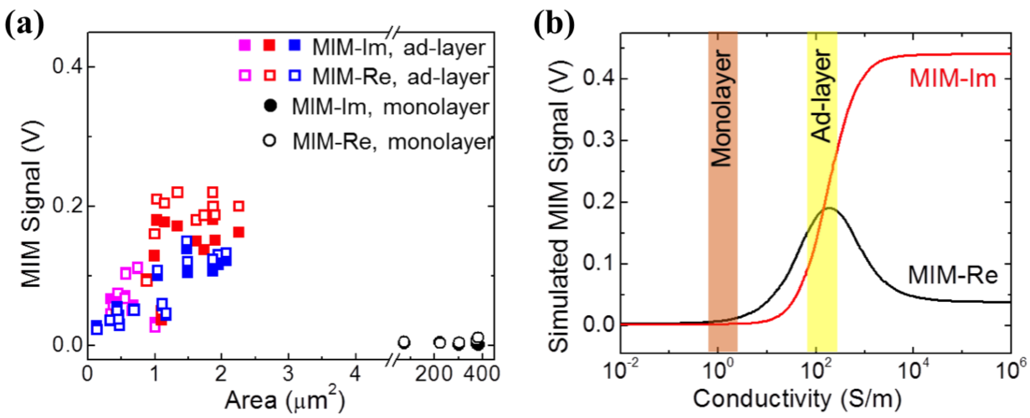

Figure 10: (a) MIM-Im signals versus sample area of multiple flakes. (b) Simulation of MIM-Im signals versus sample conductivity.

As summarized in Figure 10 (a) [1], the strength of MIM-Im and MIM-Re signals of individual dendritic structures roughly show a linear dependence on area. However, as plotted on the same graph, the MIM signals on the monolayer are independent of the domain sizes.

A numerical simulation has been performed for quantitative understanding of the dendritic precipitates and monolayer MoS_2. Unfortunately, it is not easy to quantify the sample conductivity (σ) with high accuracy because of the complicated near-field interaction and scattered data points. However, an order of magnitude estimate of the local conductivity can be achieved within the measurement and statistical error. As shown in Figure 10 (b)[1], the signals of monolayer MoS_2 flakes correspond to a low σ of 1~10 S/m or a sheet resistance of 10^8~10^9 Ω/square, while the signals of dendritic ad-layers indicates a much higher σ of 10^2~10^3 S/m. With high conductivity and comparable size with nano-devices, the dendritic structures should not be neglect in electronic applications.

Chapter 4: Conclusion

In this thesis, the basic principles of MIM and simulation analysis of MIM results have been demonstrated. In addition, several interesting phenomena have been revealed. Layer-dependent dielectric constant of In_2Se3, which shows a sharp change between n = 4 and n = 5, have been found. For MoS_2, dendritic structures on monolayer are shown to have much higher conductivity than monolayer itself. More interesting projects about modification and characterization of electrical properties of 2D system are ongoing now and hopefully they are going to reveal more truths of nature.

References

[1] Liu, Y.; Ghosh, R.; Wu, D.; Ismach, A.; Ruoff, R.; Lai, K. Mesoscale Imperfections in MoS_2 Atomic Layers Grown by a Vapor Transport Technique. *Nano Lett.* **2014**, 14, 4682-4686.

[2] Kundhikanjana, W. Imaging Nanoscale Electronic Inhomogeneity with Microwave Impedance Microscopy. *Doctor Dissertation.* **2013**

[3] Han, G.; Chen, Z.-G.; Drennan, J.; Zou, J. Indium Selenides: Structural Characteristics, Synthesis and Their Thermoelectric Performances. *Small* **2014**, 10，2747－2765

[4] Lin, M.; Wu, Di.; Zhou, Y.; Huang, W.; Jiang, W.; Zheng, W.; Zhao, S.; Jin, C.; Guo, Y.; Peng, H.; Liu, Z. Indium Selenides: Structural Characteristics, Synthesis and Their Thermoelectric Performances. *J. Am. Chem. Soc.* **2013**, 135，13274－13277

[5] Kambas, K.; Spyridelis, J. Far infrared optical study of α-In_2Se_3 compound, Mater. Res. Bull. **1978**, 13, 653–660.

[6] Bertolazzi, S.; Krasnozhon, D.; Kis, A. Nonvolatile Memory Cells Based on MoS_2/Graphene Heterostructures. *ACS Nano* **2013**, 7, 3246–3252.

[7] Yin, Z.; Li, H.; Li, H.; Jiang, L.; Shi, Y.; Sun, Y.; Lu, G.; Zhang, Q.; Chen, X.; Zhang, H. Single-Layer MoS_2 Phototransistors. *ACS Nano* **2012**, 6, 74–80.

[8] Lopez-Sanchez, O.; Lembke, D.; Kayci, M.; Radenovic, A.; Kis, A. Ultrasensitive photodetectors based on monolayer MoS_2. *Nat. Nanotech*. **2013**, 8, 497–501.

[9] Radisavljevic, B.; Radenovic, A.; Brivio, J.; Giacometti, V.; Kis, A. Single-layer MoS_2 transistors. *Nat. Nanotech.* **2011**, 6, 147–150.

[10] Ghatak, S.; Pal, A. N.; Ghosh, A. Nature of Electronic States in Atomically Thin MoS_2 Field-Effect Transistors. *ACS Nano*, **2011**, 5, 7707–7712.

[11] Radisavljevic, B.; Kis, A. Mobility engineering and a metal–insulator transition in monolayer MoS_2. *Nat. Mater.* **2013**, 12, 815–820.

[12] Late, D. J.; Liu, B.; Ramakrishna Matte, H. S. S.; Dravid, V. P.; Rao, C. N. R. Hysteresis in Single-Layer MoS_2 Field Effect Transistors. *ACS Nano* **2012**, 6, 5635–5641.

[13] Lee, Y.-H.; Zhang, X.-Q.; Zhang, W.; Chang, M.-T.; Lin, C.-T.; Chang, K.-D.; Yu, Y.-C.; Wang, J. T.-W.; Chang, C.-S.; Li, L.-J.; Lin, T.-W. “Synthesis of Large-Area MoS_2 Atomic Layers with Chemical Vapor Deposition”. *Adv. Mater.* **2012**, *24*, 2320–2325.